Mon. Not. R. astr. Soc. (1985) **216,** 1057–1071

The late infrared development of Nova Serpentis 1970

R. M. Mitchell and G. Robinson *School of Physics (RAAF Academy), University of Melbourne, Parkville, Victoria 3052, Australia*

A. R. Hyland *Mount Stromlo and Siding Spring Observatories, The Australian National University, Canberra, ACT, Australia*

G. Neugebauer *Palomar Observatory, California Institute of Technology, Pasadena, California 91125, USA*

Accepted 1985 June 20. Received 1985 May 29; in original form 1985 March 4

Summary. Broad-band infrared observations of FH Ser (Nova Ser 1970) covering the period 40 to 529 days after discovery are presented. Strong quantitative evidence for grain growth in the period 60–111 days is derived from the agreement between predictions of dust shell models and the observations. Between days 111 and 129 the grains undergo a significant reduction in size. The infrared luminosity is found to fall as t^{-3} for $t \gtrsim 100$ days. However, up until day 200 this is due to a continuing grain size reduction, while the bolometric luminosity remains approximately constant. After day 200 the bolometric luminosity falls off as $\sim t^{-1}$. At late times, an excess flux in the 1–3 μm region appears above the dominant cool dust emission component. This excess flux is probably due to increasing line emission in the J, H and K bandpasses as the ejected shell expands.

1 Introduction

The nova now known as FH Serpentis was discovered on 1970 February 13 by Honda (1970). The recorded behaviour of this object has been of crucial significance in defining our present understanding of the energy budget in classical nova events, being the first for which significant infrared emission was discovered. Although its visual light curve (Burkhead, Penhallow & Honeycutt 1971) was unremarkable, resembling those of previous medium speed novae, infrared observations by Hyland & Neugebauer (1970) and Geisel, Kleinmann & Low (1970, hereafter GKL) revealed the commencement of infrared emission about 60 days after discovery, coincident with the rapid decline in visual light signalling the onset of the transition period. By day 90★ the infrared luminosity was approximately equal to the inferred total luminosity at visual maximum, and prior ultraviolet satellite observations in the period up to 57 days (Gallagher & Code 1974) confirmed the continuation of the total luminosity at its outburst level. The existence of a

★ All times quoted are with respect to the discovery date.

post-maximum luminosity plateau is an important ingredient of the optically thick wind model of Bath & Shaviv (1976) which deals with the basic ejection mechanism in classical novae. Unfortunately, the latest published infrared observations (GKL) ended on day 111, preventing any definite conclusion to date regarding the termination of this phase.

Since the advent of FH Ser, infrared observations of many novae have been carried out, an overview of which has been given by Bode & Evans (1983). These authors have proposed the classification of novae into classes X, Y and Z, distinguished primarily by the strength of the infrared excess. FH Ser, for which the infrared luminosity approximates that of the underlying object, clearly belongs to class X, other well-observed members of which are Nova Vul 1976 (NQ Vul) and Nova Ser 1978 (LW Ser). Ney & Hatfield (1978) monitored the infrared emission of NQ Vul for approximately 240 days after maximum, and found evidence for blackbody-like emission from dust, the effective temperature of which remained near 900 K during the interval from day 80 to day 220. Gehrz *et al.* (1980) obtained similar results for LW Ser, but were able to identify a period of grain destruction following infrared maximum. A re-analysis of the infrared development of NQ Vul by Mitchell, Evans & Bode (1983, hereafter MEB) using sophisticated dust models provided strong evidence for a post-maximum period of grain destruction in this nova as well.

Models for the infrared excess from novae have followed from two different hypotheses:

(i) Emission from dust grains which nucleate and grow from the gaseous ejecta.
(ii) Emission from pre-existing dust grains.

The latter hypothesis was put forward by Bode & Evans (1980), and requires the nova to be surrounded by a pre-existing shell of small ($\sim 0.01\,\mu$m) distant (10^{16}–10^{17} cm) graphite grains whose opacity is characterized by bands of strong absorption in the ultraviolet. As the energy distribution of the central object is known to harden with time as the ejecta expand (Bath & Shaviv 1976), eventually the peak primary emission will coincide with the absorption bands causing grain heating and the commencement of infrared emission. Discussions of the relative merits of this model vis à vis the grain growth model have been given by Bode & Evans (1981, 1983). Two key pieces of evidence weighing heavily against this interpretation are: (i) The suppression of the red wings of emission lines observed during the transition period (see e.g. Hutchings & Fisher 1973 or Smith, Noah & Cottrell 1979) which implies that the gas and dust components are intermixed, contrary to the uniform extinction predicted from a distant, pre-existing shell; and (ii) changes in *UBV* polarization (both strength and position angle) found by Piirola & Korhonen (1979) to be correlated with the infrared emission of Nova Cygni 1978.

The alternative hypothesis of contemporary grain formation and growth follows naturally from the coincidence of the onset of infrared emission with the steep drop in visual light during transition. Clayton & Wickramasinghe (1976, hereafter CW) developed a model based on the nucleation and growth of graphite grains. They predicted an initial period of relatively rapid grain growth which was broadly able to account for the early steep decline in grain temperature inferred from the infrared observations.

In this paper we present hitherto unpublished infrared observations of FH Ser, resulting from a continuation of the observing programme of Hyland & Neugebauer (1970). These observations are then analysed in detail using procedures based on the grain growth model of CW.

2 Observations

The new data for FH Ser presented here were obtained between 1970 May 8 and 1971 July 27 using the Mount Wilson 60- and 100-inch telescopes, and the 200-inch Hale telescope. The observed infrared magnitudes at J (effective wavelength $1.25\,\mu$m), H ($1.65\,\mu$m), K ($2.2\,\mu$m), L

Table 1. Observed infrared magnitudes of FH Ser.*

DAY†	[J]	[H]	[K]	[L]	[M]	[N]
40	...	...	+6.18(06)§	...	...	...
68	+5.06(15)	+3.29(10)	+1.53(06)	-0.52(07)	-1.56(10)	...
69	+5.31(10)	+3.47(06)	+1.58(06)	-0.55(07)	-1.55(10)	...
70	+5.39(08)	+3.48(05)	+1.61(05)	-0.54(05)	...	-2.79(07)
84	+6.36(09)	+4.08(06)	+1.93(06)	-0.66(06)	...	...
85	+6.62(39)	+4.13(06)	+1.99(06)	-0.69(05)	...	...
88	+6.64(08)	+4.29(11)	+2.01(11)	-0.66(06)	-1.83(09)	...
89	+6.81(08)	+4.33(09)	+2.07(08)	-0.58(06)	...	-3.41(10)
90	+6.72(26)	+4.41(09)	+2.10(08)	-0.58(06)	-1.85(07)	...
91	+6.59(15)	+4.54(06)	+2.28(05)	-0.52(05)	...	-3.43(11)
92	+6.83(15)	+4.60(06)	+2.27(04)	-0.51(05)	-1.81(07)	...
129	...	+4.82(06)	+2.49(05)	-0.30(07)	...	...
151	...	+4.94(06)	+2.70(05)	-0.05(06)	...	...
152	...	+4.99(06)	+2.72(05)	-0.02(05)	...	...
154	+8.20(100)	+5.14(07)	+2.76(05)	+0.05(07)	-0.69(11)	...
156	...	+4.86(07)	+2.58(08)	...	-0.88(07)	...
183	+7.97(20)	+5.54(13)	+3.14(12)	...	-0.42(14)	...
210	+7.42(100)	+5.97(20)	+3.70(12)	+1.21(13)	...	-1.90(15)
212	...	+5.83(05)	+3.72(04)	...	-0.06(16)	...
216	...	+6.25(06)	+3.88(05)	+1.28(05)	...	...
240	...	+7.74(67)	+4.76(07)	+1.93(10)	+0.95(22)	...
245	...	+6.97(06)	+4.69(05)	+2.06(06)	...	...
386	...	+9.72(23)	+8.20(09)	+5.16(09)	...	...
395	...	...	+8.90(49)	+5.85(65)	...	-0.60(12)
397	...	+9.77(15)	+8.06(05)	...	...	...
440	...	...	...	...	+2.35(100)	+0.71(14)
442	...	10.51(24)	+9.05(11)	...	...	...
503	...	...	...	...	+5.65(24)	+0.77(12)
529	...	11.31(15)	10.01(10)	+7.72(19)	...	...

* Magnitudes for days 40, 68, 69 and 70 were previously presented by Hyland & Neugebauer (1970), the slight adjustments to the results for day 70 being due to further analysis of the data.

† Time is expressed relative to the discovery date of the nova, the 13th February 1970 (JD 2440631).

§ Numbers in parentheses indicate uncertainty in hundredths of a magnitude.

(3.5 μm), M (4.8 μm) and N (10.1 μm) are presented in Table 1 together with uncertainties in the observations. The photometer and photometric system appropriate to these observations have been described by Becklin & Neugebauer (1968) and Hyland *et al.* (1969). Fluxes may be obtained from the tabulated magnitudes using the absolute calibration given by Wilson *et al.* (1972).

3 Results

3.1 INFRARED LIGHT CURVES

The infrared light curves of FH Ser, derived from the data of Table 1 and the observations of GKL are shown in Fig. 1, together with curves based on models which will be presented in Section 4 below. The observed characteristics of the light curves may be divided as follows:

(i) During the early part of the dust phase, $70 \lesssim t \lesssim 111$ days, the light curves fade steeply at the short wavelengths (J, H and K), less steeply at L, and actually *brighten* at M and N.

(ii) Somewhere between days 111 and 129 a surprising event takes place which causes a marked discontinuity in the light curves at H, K and L (the data are deficient in the other bands). This discontinuity is most pronounced at K, where the light curve brightens by $\sim$0.7 mag during this interval.

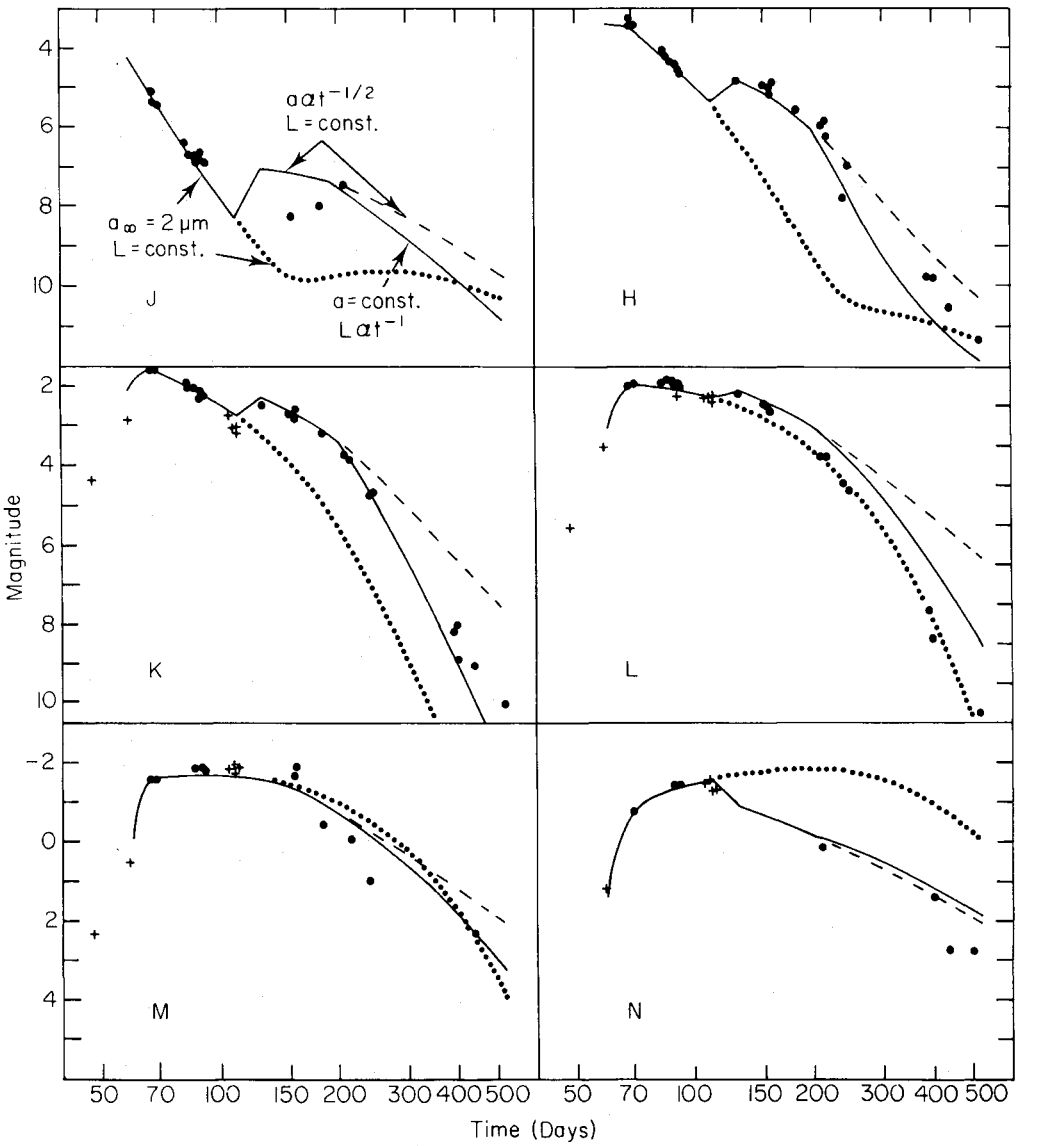

Figure 1. Infrared light curves of FH Ser. The filled circles represent the observations presented in this work, while the crosses were derived from the data of Geisel *et al.* (1970). At *K* and *L* the fluxes of Geisel *et al.* were converted to relative magnitudes normalized to our data on day 90, when observations using both systems were made. No simultaneous observations exist at *M* and *N*; here we have converted the fluxes of Geisel *et al.* to our magnitude scale using the absolute calibration of Wilson *et al.* (1972). The lines represent theoretical light curves predicted from the dust models described in Section 4. The solid line corresponds to the best piecewise fit of the infrared light curves of FH Ser. The dotted line shows the result of continuing grain growth beyond day 111, while the dashed line indicates the light curve corresponding to constant bolometric luminosity and continued grain size reduction beyond day 200.

(iii) Following this event, fading occurs in all bands except *J*; however, the significance of the *J* result is weakened by the large errors and lack of data at this wavelength.

The implications of these data regarding effective dust temperatures are shown in Fig. 2, in which colour temperatures derived from the *H*–*K*, *K*–*L* and *K*–*N* colour indices are plotted against time. All temperatures show a decline ~200 K in the pre-infrared maximum stage (i.e. up to day 90; see Section 4.3.1 below), resulting from a combination of cooling due to expansion and grain growth (since the infrared emission efficiency increases with grain size). The subsequent discontinuity in the near-infrared light curves noted above appears as an increase in dust

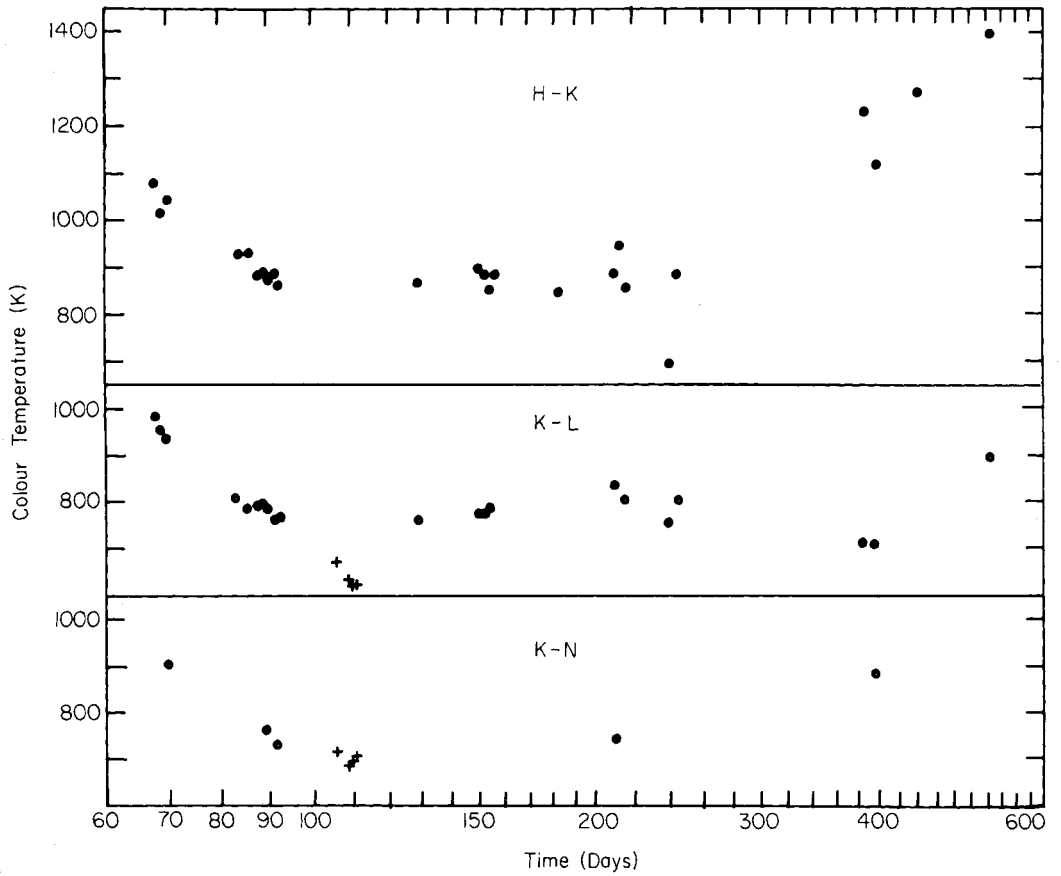

Figure 2. Time development of the $H-K$, $K-L$ and $K-N$ colour temperatures of FH Ser. Filled circles: this work; crosses: derived from the data of Geisel *et al.* (1970).

temperature between days 111 and 129. At later times ($129 \leqslant t \leqslant 240$ days) the colour temperature does *not* fall as expected (constant velocity optically thin blackbody expansion predicts $T \propto t^{-1/2}$) but remains in the range 700–900 K. This behaviour is similar to the 'isothermal dust phase' of NQ Vul found by Ney & Hatfield (1978) except that the temperature rise preceding it is far more pronounced in FH Ser.

The small amount of data later than 300 days shows some evidence for a rise in effective temperature 400–500 days after outburst. This most unexpected result contrasts with the monotonic decline in temperature found by Ney & Hatfield (1978) for NQ Vul at late times.

3.2 DEVELOPMENT OF THE INFRARED ENERGY DISTRIBUTION

In order to illustrate the development of the dust radiation, energy distributions have been plotted at six epochs for which reasonable spectral coverage is available, as shown in Fig. 3. Approximate blackbody fits to the data are also shown.

From day 70 to day 91 the effective dust temperature is seen to fall by approximately 200 K, in general agreement with the behaviour of the light curves noted above. The discontinuity in the light curves in the interval 111–129 days is reflected in the marginal *rise* in effective dust temperature from day 91 to day 154. At subsequent epochs it becomes increasingly difficult to fit the data using a single temperature blackbody. Instead, the energy distribution may be characterized by a cool blackbody component superimposed on which is an excess in the 1–3 μm region. The cool component, which is responsible for the bulk of the infrared luminosity,

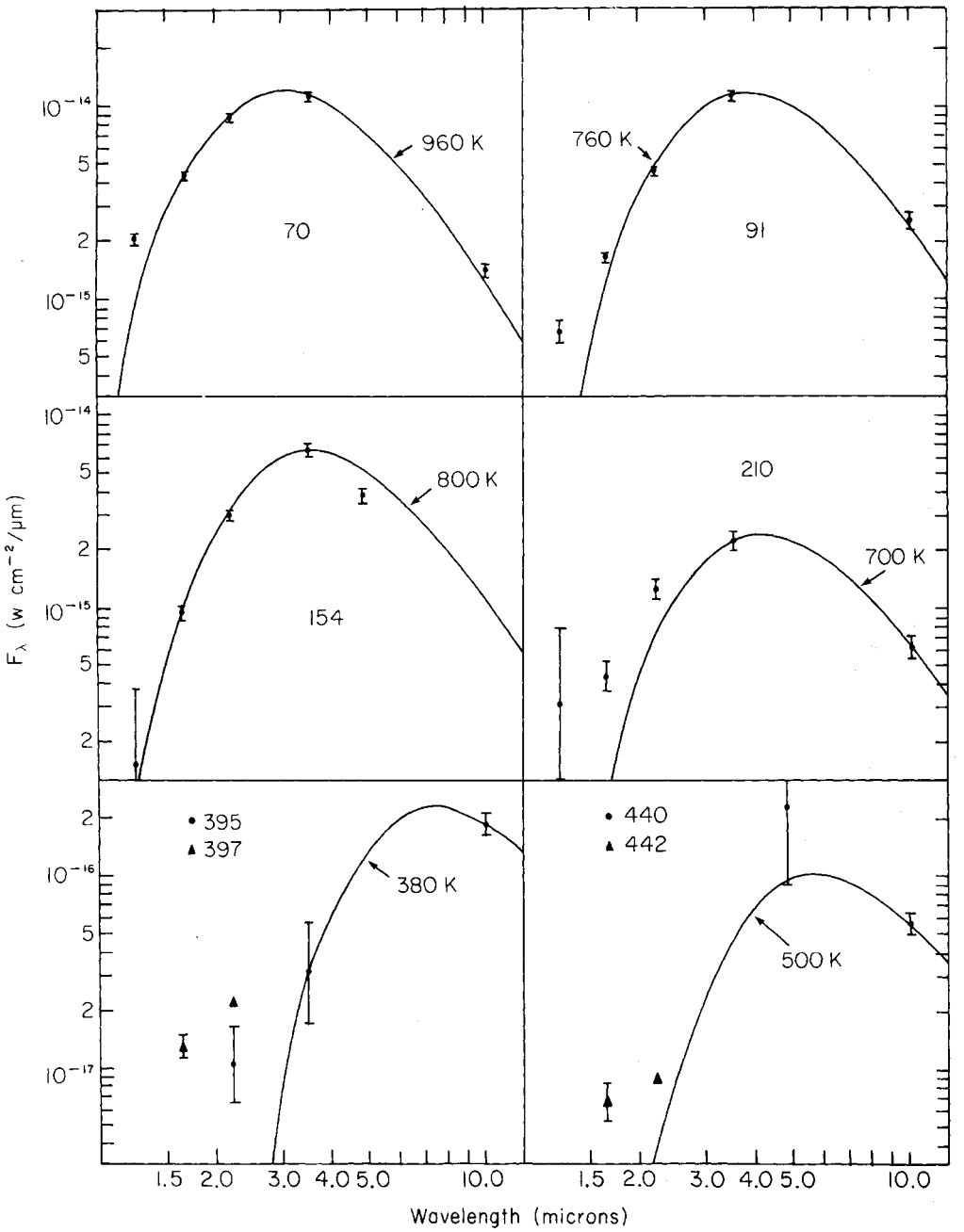

Figure 3. Representative energy distributions of FH Ser, together with approximate blackbody fits. Note the marked decrease in effective temperature between days 70 and 91, and the marginal *increase* from day 91 to day 154. Beyond day 210 the energy distribution broadens due to excess emission in the 1–3 μm region appearing above the cool dust emission component.

decreases in temperature from ~700 K on day 210 to 400–500 K after day 400, whilst the short-wavelength excess increases in relative strength and becomes bluer over the same period.

The recognition of this two-component characteristic readily explains the increase in colour temperature at late times seen in Fig. 2. The $H-K$ colour measures the short-wavelength excess and therefore records the highest temperature, while the $K-L$ and $K-N$ colours include progressively more of the cool component.

4 Grain growth model for FH Ser

As previously mentioned, CW developed a model which was fitted to some of the observed properties of FH Ser. The model was based on the rapid formation of a fixed number of carbon nucleation centres which subsequently grow due to accretion of further carbon atoms according to simple kinetic theory. The resulting dependence of grain size on time is

$$a(t)=a_0+a_\infty\left\{1-\left(\frac{t}{t_d}\right)^{-5/4}\right\} \tag{1}$$

where a_0 is the nucleation size, a_∞ the limiting grain size and t_d is the dust condensation time. CW found that the infrared behaviour of FH Ser up to day 111 required $t_d\sim45$ days and $a_\infty\sim2\mu$m. In the following we extend and modify the method of CW to represent the evolution of FH Ser over the wider period of time covered by our observations.

4.1 DEVELOPMENT OF THE DUST OPTICAL DEPTH

MEB initiated the quantitative investigation of the time dependence of optical depth in their discussion of NQ Vul. In particular, they compared the 'empirical' optical depth, defined by the extinction required to attenuate an assumed intrinsic visual light curve to the observed level, with a 'theoretical' function found by integrating the assumed dust opacity through the shell. Their approach took no account of grain growth and was therefore unable to represent the observations prior to infrared maximum; however, a discrepancy between the empirical and theoretical functions at later times was an important result which they interpreted as evidence for grain destruction following the infrared maximum. Here we apply a similar method to FH Ser, but extend it to cover the grain growth period as well.

Computation of the empirical optical depth follows from

$$\tau_V^{\rm emp}(t)=\frac{m_V^{\rm obs}(t)-m_V^{\rm int}(t)}{1.086} \tag{2}$$

where $m_V^{\rm obs}(t)$ and $m_V^{\rm int}(t)$ are respectively the observed and assumed intrinsic visual magnitudes. In order to compute the latter we have adopted the method of Kwok (1983) who showed that the pre-transition visual light curve of FH Ser can be well matched by the predictions of the optically thick wind model of Bath & Shaviv (1976) when modified to incorporate a mass-loss rate which dries up according to the power law $\dot{M}(t)=\dot{M}_0(t_0/t)^\alpha$, where $\dot{M}_0$ is the outburst mass-loss rate and t_0 is a scaling time. Kwok found that suitable parameters for FH Ser are $\dot{M}_0=10^{-4}M_\odot\,{\rm yr}^{-1}$, $t_0=0.1$ yr and $\alpha=2$. In the optically thick wind model the decline in visual light is a consequence of the increasing effective temperature of the photosphere as the ejected shell expands, coupled with the constraint of constant bolometric luminosity.

The observed visual light curve required to compute $\tau_V^{\rm emp}(t)$ from equation (2) has been taken from Burkhead *et al.* (1971). The resulting function is plotted in Fig. 4 where it is compared with other functions described below.

If the grain radius $a(r,t)$ and grain number density distribution $n_{\rm dust}(r,t)$ are known functions, the 'theoretical' optical depth may be found from

$$\tau_\lambda^{\rm th}(t)=\int_{R_{\rm min}}^{R_{\rm max}}Q_\lambda^{\rm ext}[a(r,t)]\pi a^2(r,t)n_{\rm dust}(r,t)dr. \tag{3}$$

For consistency with the foregoing, $a(r,t)$ and $n_{\rm dust}(r,t)$ are found by assuming the power-law decline of mass-loss rate with time used in computing $m_V^{\rm int}(t)$. This leads to a gas-phase number

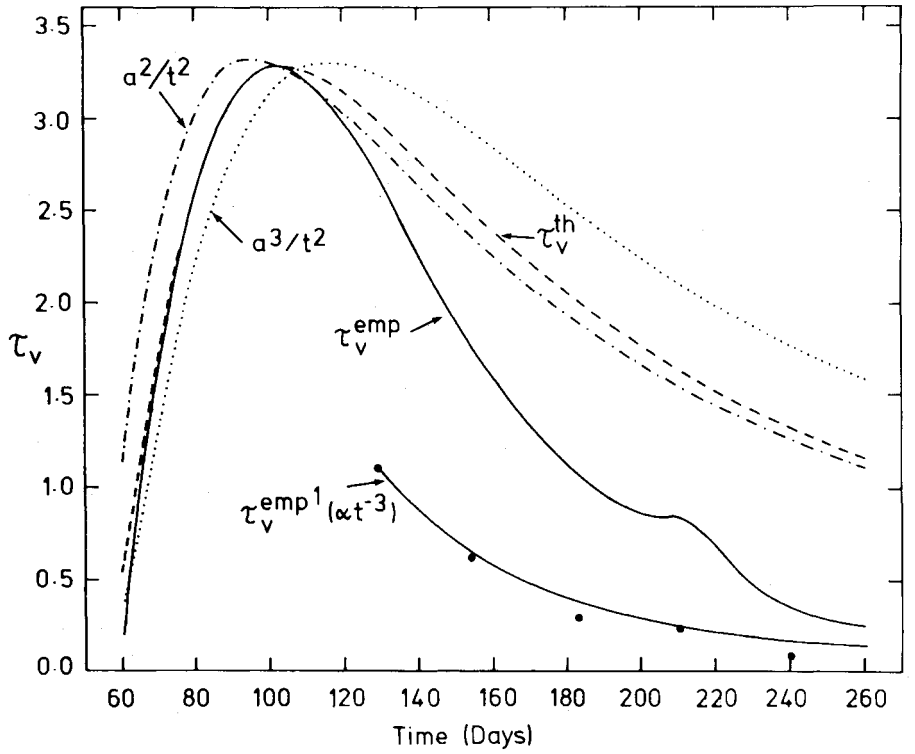

Figure 4. Time dependence of visual optical depth. The solid line labelled τ_V^{emp} indicates the empirical optical depth derived from the difference between the observed light curve and an assumed intrinsic light curve. The dashed line represents the theoretical optical depth function derived by assuming continued grain growth in an extended shell. The dot–dashed and dotted curves correspond to the functions a^2/t^2 and a^3/t^2, appropriate to a thin shell with grain growth where the absorption efficiency is respectively constant or increasing linearly with grain size. The filled circles were derived from the observed behaviour of the infrared luminosity (see Fig. 5). The function $\tau_V^{emp'}$ is a simple t^{-3} law fitted to the day 129 point.

density distribution of the form

$$n_{gas}(r,t) \propto r^{-2}\left(\frac{vt_0}{vt-r+r_0}\right)^{\alpha} \tag{4}$$

where v is the expansion velocity and r_0 is the radius of the system at time t_0 (see Kwok 1983). Note that our adoption of a physically extended shell differs from the thin shell assumption of CW. Since grain nucleation is a binary process, the number density of nucleation centres varies as the square of the gas density at the nucleation radius, R_{min}. Given that a grain at (r,t) passed through R_{min} at time $t_{min}=t-(r-R_{min})/v$, this leads to the grain number density distribution

$$n_{dust}(r,t) \propto r^{-2}\left(\frac{vt_0}{vt-r+r_0}\right)^{2\alpha}. \tag{5}$$

Following CW, the grain growth rate by accretion of gas-phase carbon monomers may be written as

$$\frac{da(r,t)}{dt} \propto n_c(r,t)T_{gas}^{1/2}(r) \tag{6}$$

where $n_c(r,t)$ is the carbon monomer density and $T_{gas}(r)$ is the gas kinetic temperature. Assuming

$n_c(r,t) \propto n_{gas}(r,t)$ and $T_{gas}(r) \propto r^{-1/2}$, equation (6) may be integrated to give

$$a(r,t) = a_0 + a_\infty(t_{min}) \left\{ 1 - \left(\frac{R_{min}}{r} \right)^{5/4} \right\} \tag{7}$$

where $a_\infty(t_{min})$ is the limiting size for grains at (r,t) whose nucleation at R_{min} took place at time t_{min}. Equation (7) is practically identical to equation (1) above taken from CW except that in the latter's thin shell model a_∞ was single-valued. In our case $a_\infty(t_{min})$ is linearly related to the gas density at R_{min}, i.e. $a_\infty(t_{min}) \propto n_{gas}(R_{min}, t_{min})$, and hence, from equation (4) we may write

$$a_\infty(t_{min}) = \beta \left(\frac{vt_0}{vt - r + r_0} \right)^\alpha \tag{8}$$

where β is a constant which is fixed by specifying the grain size at the outer boundary at a particular time. An expression for the optical depth may now be obtained by substituting equations (5), (7) and (8) into equation (3), which becomes

$$\tau_V^{th}(t) \propto \frac{1}{R_{max}} \int_{x_{min}}^{1} \left[a_0 + \beta \left(\frac{x_0}{1 + x_0 - x} \right)^\alpha \left\{ 1 - \left(\frac{x_{min}}{x} \right)^{5/4} \right\} \right]^2 x^{-2} \left(\frac{x_0}{1 + x_0 - x} \right)^{2\alpha} dx \tag{9}$$

where $x = r/R_{max}$, $x_{min} = R_{min}/R_{max} = t_d/t$ and $x_0 = vt_0/R_{max} = t_0/t$. We have evaluated this integral as a function of time for the following parameters: $t_0 = 36.5$ days (from Kwok 1983); $t_d = 50$ days; $a_0 = 0.003\,\mu$m (from CW) and $\beta = 0.5$–$2.0\,\mu$m. The results were found not to be critically dependent on the value of β.

A comparison between the empirical and theoretical optical depth functions is shown in Fig. 4, where the maximum value of τ_V^{th}, which occurred at ~105 days has been normalized to the peak value of $\tau_V^{emp} = 3.3$ which occurred at ~100 days. Also shown in Fig. 4 are similarly normalized functions proportional (respectively) to $a^3(t)/t^2$ and $a^2(t)/t^2$. Functions of this form are appropriate in the simplified model of CW where the total number of grains remains constant. The former function applies to small grains whose absorption efficiency Q_λ^{abs} increases linearly with grain size, whilst the latter applies to larger grains when Q_λ^{abs} has saturated at unity.

From Fig. 4 it may be seen that the theoretical function computed from equation (9) is in excellent agreement with the empirically derived function during the period 60–100 days, which we interpret as strong quantitative support for our variant of the grain growth model. By contrast, neither of the simple functions of CW provides satisfactory agreement. We note that the fit between τ_V^{emp} and τ_V^{th} is quite sensitive to the choice of the dust condensation time t_d, and indeed was partly responsible for our adoption of $t_d = 50$ rather than 45 days as used by CW.

At times later than ~100 days, $\tau_V^{emp}(t)$ is seen to decline more rapidly than any of the other functions. This result is qualitatively similar to that found by MEB for NQ Vul, and will be discussed further below.

4.2 ENERGETICS AND GRAIN DESTRUCTION

The optical depth computations presented above are subject to a simple check using our infrared observations since, assuming a constant absorption optical depth τ_V throughout the spectral region in which the source is emitting, the infrared luminosity emerging from the shell is given by

$$L_{IR} = L_{bol}\{1 - \exp(-\tau_V)\} \tag{10}$$

where L_{bol} is the bolometric luminosity. The time dependence of the infrared luminosity (defined as the energy radiated in the 1 to 100 μm region) has been found by integrating over wavelength energy distributions such as those shown in Fig. 3, and the results are shown in Fig. 5. The data for

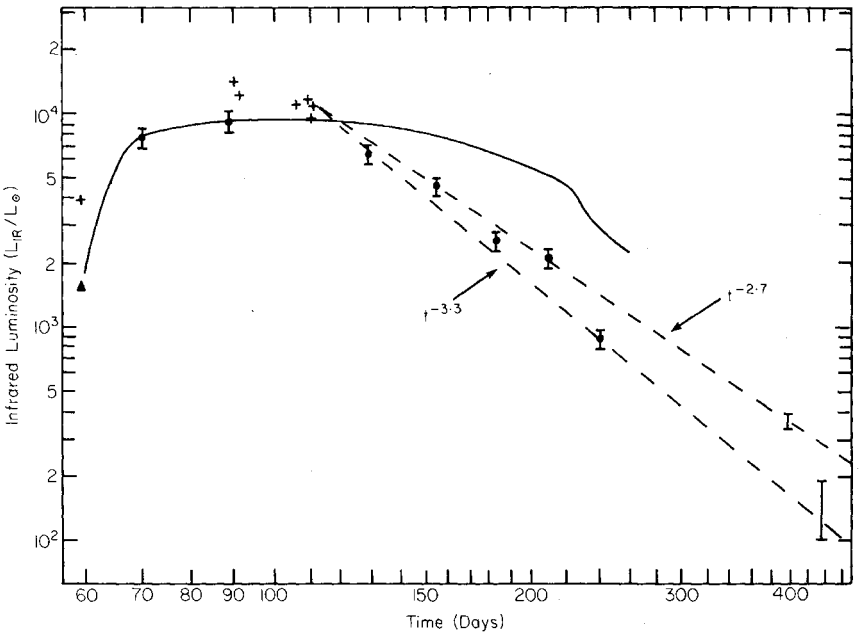

Figure 5. The time dependence of infrared luminosity for FH Ser. Filled circles with error bars: this work, obtained as described in the text; crosses: data of Geisel *et al.* (1970) scaled to a distance of 650 pc; filled triangle: computed from the observations of Geisel *et al.* excluding energy emitted shortward of 1 μm. The estimates shown with error bars on days (395/397) and (440/442) were computed by integrating normalized blackbodies over wavelength. The uncertainty indicated arises from the assumption of an effective temperature in the range 300–500 K. The solid line indicates the infrared luminosity expected if the absorption optical depth varies as τ_V^{emp} (see Fig. 4). The two dashed lines, which represent the infrared luminosity varying as $t^{-2.7}$ and $t^{-3.3}$ respectively, indicate that for $t \gtrsim 100$ days the infrared luminosity declined approximately as t^{-3}.

this diagram have been derived by direct manual integration where possible, in which case the energy distributions were extrapolated in the range $10<\lambda<100\,\mu$m using blackbody temperatures derived from the L–N or M–N colours as available. At times later than 154 days the appearance of the 1–3 μm excess may result in the computed colour temperature giving rise to a misleadingly high estimate of the dust temperature, in which case the extrapolated luminosity would be erroneously low. To allow for this possibility the effect of reducing the blackbody temperature substantially below the computed colour temperature has been investigated and found to make no more than a few per cent difference to the computed luminosity. The total error resulting from uncertainties in extrapolation and interpolation is estimated to be $\lesssim$10 per cent. In the two cases at late times shown as simple error bar estimates, the observational data were not sufficiently complete to permit manual integration. Hence blackbodies normalized at one or more wavelengths were integrated instead. In these cases the size of the error bars reflects the uncertainties in the blackbody temperature. Also plotted in Fig. 5 are the 'total' luminosity estimates of GKL normalized to a distance of 650 pc (Gallagher & Code 1974). These data apparently include an estimate of the visual luminosity, and would be expected to be in excess of L_{IR} if the visual contribution was significant. This is confirmed by our independent computation of L_{IR} on day 59 from the plotted energy distributions of GKL, which is over a factor of 2 below their value.

The essential features of the observational data of Fig. 5 are the rise toward infrared maximum on day 90 when the luminosity was $\sim 10^4 L_\odot$ (D=650 pc) followed by a monotonic decline, beginning about day 100, during which L_{IR} fell approximately as t^{-3}. Also shown in Fig. 5 is a function derived from equation (10) in which τ_V has been set equal to the empirical optical depth shown in Fig. 4. This function has been normalized to pass through our data point at day 90. Good

agreement is obtained from day 59 until day 111 excepting the data of GKL at days 90 and 91. However, beyond day 111 serious disagreement is seen in that the observed luminosity begins its t^{-3} decline whilst the function $1-\exp(-\tau_V)$ remains close to unity since, according to Fig. 4, the shell remains optically thick until about day 200. From equation (10), this must be due either to a decline in $L_{\rm bol}$ between days 111 and 129, or to an unexpectedly large decrease in τ_V over the same period. The former possibility may be ruled out by reference to Fig. 2 which shows that the dust temperature *increases* over the above time interval, contrary to the cooling which would be brought about by a luminosity decline. This points to a sharp fall in optical depth over and above that depicted in Fig. 4 for $\tau_V^{\rm emp}$. Solving equation (10) for τ_V using the observed value of $L_{\rm IR}$ on day 129 gives $\tau_V=1.11$, to be compared with $\tau_V^{\rm emp}(129)=2.66$. Computations at later times up to day 210 are well fitted by a t^{-3} variation, shown in Fig. 4 as $\tau_V^{\rm emp'}$.

The marked discrepancy between $\tau_V^{\rm emp}(t)$ and $\tau_V^{\rm emp'}(t)$ must be attributed to a breakdown in the assumption that the development of the intrinsic visual luminosity can be followed by Kwok's method into the post-transition period (see equation 1). The rapid fall-off in optical depth from days 111 to 129 implies a comparable rapidly fading intrinsic light curve. This could be produced by the envelope exhaustion discussed by Shara (1981) leading to an accelerated shrinkage of the photosphere, and corresponding increases in effective temperature and bolometric correction.

The large discrepancy between $\tau_V^{\rm th}(t)$ and $\tau_V^{\rm emp'}(t)$ seen in Fig. 4 requires a physical mechanism which not only decreases the shell optical depth but also produces an increase in grain temperature over that expected from simple constant velocity expansion (see Fig. 2). As with NQ Vul (MEB) and LW Ser (Gehrz *et al.* 1980) both requirements are satisfied if a significant grain size reduction takes place following infrared maximum.

If the grain number density is assumed unchanged, a rough estimate of the relative grain size change may be obtained by noting that, to a first approximation, $\tau \propto a^2$. Hence, the factor ~ 3 reduction in optical depth apparent from Fig. 4 on day 129 implies a factor ~ 1.7 reduction in grain size. The temporal behaviour of grain size is further considered below.

4.3 INTERPRETATION OF THE INFRARED LIGHT CURVES

A critical test of the grain growth and destruction model developed in preceding sections is whether it correctly predicts the time development of the monochromatic infrared magnitudes. To determine this, we attempted to apply the spatially extended radiative transfer model of MEB to FH Ser, using the density and grain size distributions given in Section 4.1 above. However, this approach was severely hampered by numerical problems due to the extremely wide range of opacity ($\sim 10^6$) encountered in traversing the shell of a typical model. Hence we have adopted a simpler procedure based on the isothermal model of Robinson & Hyland (1977).

In this method, the shell radius at a given time is fixed by assuming a constant expansion velocity of 700 km s^{-1} (Gallagher 1977). Then the shell temperature is found by iteratively solving the radiative balance equation. This solution depends on, among other things, the dust opacity law and the luminosity and temperature of the central source. The opacity has been assumed constant for wavelengths shorter than the 'break' wavelength $2\pi a(t)$ and to vary as λ^{-1} for $\lambda \geqslant 2\pi a(t)$, in accordance with the λ^{-1} variation found by Koike, Hasegawa & Manabe (1980) for amorphous carbon particles. The grain size time dependence is taken from equation (1) with $a_0=0.003\,\mu$m, $t_{\rm d}=50$ days and a_∞ treated as unknown.

Specification of the time development of the photospheric temperature is important since, under certain conditions, the contribution from attenuated primary radiation in the J, H and K bands was found to swamp the dust radiation. The nova wind model of Bath & Shaviv (1976) predicts $T_{\rm e} \propto \dot{M}^{-1/2}$ which, combined with Kwok's (1983) mass-loss law $\dot{M}=\dot{M}_0(t/t_0)^{-2}$ yields $T_{\rm e}(t)=T_{\rm e}(0)(t/t_0)$. Estimates of the spectral type at outburst range from F2Ia (Gallagher & Code

1974) to F8 (Walborn 1971) which suggests an initial temperature of $T_e(0) \sim 6500$ K. Using Kwok's value of $t_0 = 36.5$ days leads to a linearly increasing effective temperature which closely reproduces the hardening nova energy distribution prior to transition (see Gallagher & Code 1974). The source luminosity was taken as $1.9 \times 10^4 L_\odot$ (CW) although departures from this at late times are considered. Once the time dependence of optical depth has been specified (see below) and the shell temperature computed, it is straightforward to solve for the monochromatic output fluxes and hence to obtain light curves.

4.3.1 Grain growth period (50–110 days)

During this period the visual optical depth was taken to vary as $\tau_V^{\rm emp}$ shown in Fig. 4. Several model runs were made with values of a_∞ between 0.1 and 2.0 μm. Computations were begun at day 60 since no reliable optical depth estimates are available at earlier times.

The computed light curves are plotted together with the observations in Fig. 1, where the theoretical functions have been arbitrarily normalized to pass through the observed point at day 70 for all wavelengths. The optimal value of a_∞ was found to be 2.0 μm, in complete agreement with CW. Smaller values of a_∞ lead to the prediction of excessive brightening at 10 μm in the period 60–110 days. Substituting $a_\infty = 2.0\,\mu$m into equation (1) implies that the grains reached a size $\sim 1.3\,\mu$m by day 110.

Reference to Fig. 1 shows that excellent agreement between observed and predicted light curves is obtained during this period except at day 60, probably due to the poor determination of $\tau_V^{\rm emp}$ when $m_V^{\rm obs} \simeq m_V^{\rm int}$ (see equation 2). This agreement adds support to the already strong case for real-time grain formation and growth in nova envelopes.

4.3.2 Grain destruction period (111–129 days)

As anticipated from Section 4.2, the discontinuity in the light curves at H, K and L in the interval 111–129 days seen in Fig. 1 requires a substantial grain size reduction in the models over the same period. Light curves resulting from continuing grain growth beyond day 111 are shown in Fig. 1, where it is seen that for $\lambda < 3.5\,\mu$m the model predictions fall below the observations, while the reverse is true for $\lambda > 3.5\,\mu$m (in particular at $\lambda = 10.1\,\mu$m). Clearly this requires an increase in dust temperature from day 111 which affects all subsequent points. In order to model this we have arbitrarily reduced the value of a_∞ from its value of 2.0 μm up to day 110 to a smaller value on day 130. Best overall agreement was obtained with $a_\infty(130) = 0.5\,\mu$m. The visual optical depth on day 130 was taken as 1.1 (see Fig. 4). As seen from Fig. 1, the grain size decrease satisfactorily reproduces the brightening observed at H, K and L. The extent of the predicted brightening decreases with increasing wavelength, actually reversing to a *fading* at M and N. This occurs since the wavelength bands short of $\sim 3.5\,\mu$m are on the Wien side of the ~ 800 K dust continuum, where a temperature increase more than compensates for the decrease in optical depth. Conversely, the M and N bands are on the Rayleigh–Jeans side of the continuum which is relatively less affected by the temperature rise.

The actual grain size implied by $a_\infty(130) = 0.5\,\mu$m is 0.35 μm, a factor of 3.7 less than the grain size on day 110 ($\sim 1.3\,\mu$m). This is well in excess of the factor ~ 1.7 found from a consideration of the optical depth in Section 4.2, a discrepancy that may be a consequence of the isothermal approximation of the present models. In an optically thick, spatially extended dust shell incorporating a temperature gradient, an apparent temperature rise will be produced merely by a reduction in optical depth, which exposes hotter underlying grains to the observer. Hence less grain size reduction would be required to produce a given temperature rise. This effect was investigated by MEB and found to be significant in NQ Vul.

Alternatively, it could be argued that the temperature increase caused by a grain size reduction

would depend on the dust opacity law, and that by adopting a more steeply declining variation a given temperature increase would be produced by a smaller grain size reduction. We have investigated this possibility using a λ^{-2} law for $\lambda \geq 2\pi a(t)$, and found that although the required reduction in grain size is indeed less, the fit during the grain growth period is no longer satisfactory, regardless of the value of a_∞. More sophisticated modelling techniques are required to resolve this problem.

An estimate of the required sputtering rate may be obtained by assuming that the grains are reduced in radius by a factor $\gtrsim 1.7$ over a 20-day period. Taking an initial grain size of $1.3\,\mu$m on day 110, the resulting sputtering rate is $\gtrsim 3\times10^{-2}\,\mu\mathrm{m\,day^{-1}}$. This is higher than that found by MEB for NQ Vul ($\sim 3\times10^{-3}\,\mu\mathrm{m\,day^{-1}}$) and that predicted by Mitchell & Evans (1984) for charge-mediated chemisputtering ($\sim 7\times10^{-4}\,\mu\mathrm{m\,day^{-1}}$). Mitchell & Evans pointed out that this rate could be substantially increased by density clumping in the ejecta, a phenomenon which may also be required to promote the growth of micrometre-sized grains in the first place (Draine 1979).

The timing of the grain destruction period (111–129 days) is in good agreement with estimates of the hydrogen ionization time-scale, which range from ~100 days (Mitchell & Evans 1984) to 130 days (Gallagher 1977). This is consistent with the hypothesis of Mitchell & Evans in which the grain destruction phase is initiated by the advent of hydrogen ionization.

4.3.3 Late infrared development (t>129 days)

It was found in Section 4.2 that the infrared luminosity after day 100 varies as $\sim t^{-3}$. This may be used to constrain the system luminosity and shell optical depth in the following manner. Once the shell is optically thin ($t \gtrsim 130$ days) equation (10) reduces to $L_{\mathrm{IR}} \simeq \tau_V L_{\mathrm{bol}}$. If we assume that L_{bol} remains constant throughout the period of our observations, then it follows that $\tau_V \propto t^{-3}$ for $t \gtrsim 100$ days. However, for constant grain size, τ_V falls as t^{-2} due to inverse-square density dilution. Hence a t^{-3} variation implies a continuing grain size reduction of the form $a \propto t^{-1/2}$, since $\tau \propto a^2$. An alternative possibility is that at some time the grain size reduction ceases, after which L_{bol} must begin to decline as t^{-1} in order to maintain $L_{\mathrm{IR}} \propto t^{-3}$.

We have investigated both possibilities, and find that the former alternative (L_{bol} constant, $a \propto t^{-1/2}$) provides a satisfactory fit to the observations up until ~200 days, as seen in Fig. 1. However, at later times the model prediction declines less steeply than the observations. Accordingly, we have computed alternative light curves where the grain size remains fixed at its value on day 200 and L_{bol} falls as t^{-1}. As seen from Fig. 1, this modification overcorrects at H and K and undercorrects at longer wavelengths, but nevertheless provides a plausible description of the observed behaviour.

We note that Gallagher & Starrfield (1978) expressed uncertainty as to whether the decline in infrared luminosity found by GKL between days 90 and 111 really heralded the 'turn-off' of the nova. Our results suggest that the fall in L_{IR} up to day 200 was due to changes in the dust shell, and that the true turn-off in L_{bol} did not begin until after that time.

In Section 3.2, evidence was found for the emergence of an excess in the $1–3\,\mu$m region at late times over blackbody fits to the dust continuum (see Figs 2 and 3). Identification of this excess as due to radiation from a secondary compact dust shell is almost certainly incorrect since (a) it is difficult to see how its colour temperature could *increase* with time in accordance with Fig. 2 and (b) conditions of low density and high gas temperature characteristic of the nebulae stage of novae are unlikely to favour a late episode of grain formation.

A more likely explanation is that the fluxes in the J, H and K bandpasses are dominated by gaseous line emission beyond ~day 200. In support of this, Black & Gallagher (1976) have shown that the late $2–4\,\mu$m spectrum of Nova Cyg 1975 (V1500 Cyg) obtained by Grasdalen & Joyce (1976) can be explained by the increasing prominence of emission lines of hydrogen and helium.

Although there are marked differences between FH Ser and V1500 Cyg, in respect of the relatively high speed class and lack of comparable dust formation episode in the latter (Ennis *et al.* 1977), the development of a high-excitation emission line spectrum is a characteristic common to classical novae (e.g. McLaughlin 1960). On this model, the increase in the $H-K$ colour temperature of FH Ser at late times apparent from Fig. 2 would follow from the well-known increase in excitation during the nebular stage as the ejecta expands and the radiation field of the nova remnant hardens. Near-infrared spectrophotometry will be important in determining the origins of similar excesses found in future dusty novae.

5 Conclusions

In this paper we have presented previously unpublished observations of the late infrared development of FH Ser. The implications of these observations were examined using dust models. Our principal results are as follows:

(i) During the period 60–111 days after discovery, predictions of the time dependence of dust optical depth based on a grain nucleation and growth model agree well with an empirically derived function obtained by comparing the observed visual light curve with an intrinsic light curve derived by assuming that the mass-loss rate from the nova tails off as t^{-2}. Furthermore, the predicted infrared light curves of a simple dust shell model are in excellent agreement with observation during this phase. These results strongly support the idea of real-time grain nucleation and growth in novae envelopes.

(ii) Between days 111 and 129 a grain destruction event occurred, possibly initiated by the ionization of hydrogen, which reduced the grain size by a factor of $\gtrsim 1.7$. The implied sputtering rate ($\gtrsim 3\times10^{-2}\,\mu\mathrm{m\,day^{-1}}$) is an order of magnitude higher than that found by MEB for NQ Vul.

(iii) We find evidence that the bolometric luminosity remained approximately constant up until ~200 days after discovery. The observed fall in infrared luminosity ($L_{\mathrm{IR}} \propto t^{-3}$ after ~100 days) implies that grain erosion continued after day 129, the dependence of grain size on time being approximately $a(t) \propto t^{-1/2}$. Following the termination of the constant luminosity phase on about day 200, the bolometric luminosity fell approximately as t^{-1}.

(iv) At late times ($t \gtrsim 200$ days) an excess is observed in the J, H and K bands over blackbody curves representing the dust shell emission. This excess may be satisfactorily explained by the increasing dominance of gaseous emission lines in the nebular stage of the nova spectrum.

Acknowledgments

We wish to thank the various night assistants at Mount Wilson and Palomar for their help during the period of these observations. We also thank the numerous Caltech students who assisted in obtaining the observations, enabling us to get the long time coverage reported in this paper. The suggestions of an anonymous referee are gratefully acknowledged. RMM is the holder of a University of Melbourne Research Fellowship. The infrared astronomy project at the University of Melbourne is supported in part by a grant from the Australian Research Grants Scheme whilst infrared astrophysics at Caltech is supported by a grant from NSF.

References

Bath, G. T. & Shaviv, G., 1976. *Mon. Not. R. astr. Soc.*, **175**, 305.
Becklin, E. E. & Neugebauer, G., 1968. *Astrophys. J.*, **151**, 145.
Black, J. H. & Gallagher, J. S., 1976. *Nature*, **261**, 296.
Bode, M. F. & Evans, A., 1980. *Astr. Astrophys.*, **89**, 158.

Bode, M. F. & Evans, A., 1981. *Mon. Not. R. astr. Soc.*, **197,** 1055.
Bode, M. F. & Evans, A., 1983. *Q. Jl R. astr. Soc.*, **24,** 83.
Burkhead, M. S., Penhallow, W. S. & Honeycutt, R. K., 1971. *Publs astr. Soc. Pacif.*, **83,** 338.
Clayton, D. D. & Wickramasinghe, N. C., 1976. *Astrophys. Space Sci.*, **42,** 463 (CW).
Draine, B. T., 1979. *Astrophys. Space Sci.*, **65,** 313.
Ennis, D., Becklin, E. E., Beckwith, S., Elias, J., Gatley, I., Matthews, K., Neugebauer, G. & Willner, S. P., 1977. *Astrophys. J.*, **214,** 478.
Gallagher, J. S., 1977. *Astr. J.*, **82,** 209.
Gallagher, J. S. & Code, A. D., 1974. *Astrophys. J.*, **189,** 303.
Gallagher, J. S. & Starrfield, S., 1978. *Ann. Rev. Astr. Astrophys.*, **16,** 171.
Gehrz, R. D., Grasdalen, G. L., Hackwell, J. A. & Ney, E. P., 1980. *Astrophys. J.*, **237,** 855.
Geisel, S. L., Kleinmann, D. E. & Low, F. J., 1970. *Astrophys. J. Lett.*, **161,** L101 (GKL).
Grasdalen, G. L. & Joyce, R. R., 1976. *Nature*, **259,** 187.
Honda, M., 1970. *IAU Circ. No. 2212.*
Hutchings, J. B. & Fisher, W. A., 1973. *Publs astr. Soc. Pacif.*, **85,** 122.
Hyland, A. R., Becklin, E. E., Neugebauer, G. & Wallerstein, G., 1969. *Astrophys. J.*, **158,** 619.
Hyland, A. R. & Neugebauer, G., 1970. *Astrophys. J. Lett.*, **160,** L77.
Koike, C., Hasegawa, H. & Manabe, A., 1980. *Astrophys. Space Sci.*, **67,** 495.
Kwok, S., 1983. *Mon. Not. R. astr. Soc.*, **202,** 1149.
McLaughlin, D. B., 1960. In: *Stellar Atmospheres, Stars and Stellar Systems*, Vol. VI, p. 585, ed. Greenstein, J. L., University of Chicago Press, Chicago.
Mitchell, R. M. & Evans, A., 1984. *Mon. Not. R. astr. Soc.*, **209,** 945.
Mitchell, R. M., Evans, A. & Bode, M. F., 1983. *Mon. Not. R. astr. Soc.*, **205,** 1141 (MEB).
Ney, E. P. & Hatfield, B. F., 1978. *Astrophys. J. Lett.*, **219,** L111.
Piirola, V. & Korhonen, T., 1979. *Astr. Astrophys.*, **79,** 254.
Robinson, G. & Hyland, A. R., 1977. *Mon. Not. R. astr. Soc.*, **180,** 495.
Shara, M. M., 1981. *Astrophys. J.*, **243,** 926.
Smith, S. E., Noah, P. V. & Cottrell, M. J., 1979. *Publs astr. Soc. Pacif.*, **91,** 775.
Walborn, N. R., 1971. *Publs astr. Soc. Pacif.*, **83,** 813.
Wilson, W. J., Schwartz, P. R., Neugebauer, G., Harvey, P. M. & Becklin, E. E., 1972. *Astrophys. J.*, **177,** 523.